Pentacoordinate cobalt(ii) single ion magnets with pendant alkyl chains: shall we go for chloride or bromide?

Jana Juráková, Jana Dubnická Midlíková, Jakub Hrubý, Andrii Kliuikov, Vinicius Tadeu Santana, Ján Pavlik, Ján Moncoľ, Erik Čižmár, Milan Orlita, Ivan Mohelský, et al.

Pentacoordinate Cobalt(II) Single Ion Magnets with Pendant Alkyl Chains: Shall We Go for Chloride or Bromide?

Jana Juráková,[a] Jana Dubnická Midlíková,[a] Jakub Hrubý,[a] Andrii Kliuikov,[b] Vinicius Santana,[a] Ján Pavlik,[c] Ján Moncoľ,[c] Erik Čižmár,[b] Milan Orlita,[d] Ivan Mohelský,[d] Petr Neugebauer,[a] Denis Gentili,[e] Massimiliano Cavallini,[e] Ivan Šalitroš[acf*]

a) Central European Institute of Technology, Brno University of Technology, Purkyňova 123, 61200 Brno Czech Republic

b) Institute of Physics, Faculty of Science, P.J. Šafárik University Park Angelinum 9, 04154 Košice, Slovakia

c) Department of Inorganic Chemistry, Faculty of Chemical and Food Technology, Slovak University of Technology in Bratislava. Bratislava SK-81237, Slovakia. *e-mail: ivan.salitros@stuba.sk

d) LNCMI-EMFL, CNRS UPR3228, Univ. Grenoble Alpes, Univ. Toulouse, Univ. Toulouse 3, INSA-T, Grenoble and Toulouse, France.

e) Consiglio Nazionale delle Ricerche, Istituto per lo Studio dei Materiali Nanostrutturati (CNR-ISMN) Via P. Gobetti 101, 40129 Bologna, Italy.

f) Department of Inorganic Chemistry, Faculty of Science, Palacký University, 17. listopadu 12, 771 46 Olomouc, Czech Republic

Abstract

Four pentacoordinate complexes **1**-**4** of the type $[Co(L1)X_2]$ and $[Co(L2)X_2]$ (where L1=2,6-bis(1-octyl-1H-benzimidazol-2-yl)pyridine for **1** and **2**, L2=2,6-bis(1-dodecyl-1H-benzimidazol -2-yl)-pyridine for **3** and **4**; X = Cl^- for **1** and **3**, X = Br^- for **2** and **4**) have been synthesized, and their structures have been determined by X-ray analysis. The DC magnetic investigation confirmed high-spin and anisotropic behavior of metal centers of reported compounds and magnetic data were analyzed with respect to spin and Griffith-Figgis Hamiltonian. *Ab initio* analysis enabled us to identify the triaxial magnetic anisotropy for **1** and **2** and axial anisotropy for **3** and **4**, and discuss thoroughly their relation between geometry and orbital ordering. Extracted *g*-tensor components of the ground Kramers doublet from EPR spectroscopy are compatible with this prediction of magnetic anisotropy. Simulated FIRMS experimental data of **2**, **3** and **4** shows a very good agreement with theoretical calculations and provide precise values of the zero-field splitting. The AC susceptibility measurements confirmed that reported complexes are field-induced single-ion magnets. The slow relaxation of magnetization in **1** and **2** is mediated through two relaxation channels that are unusually close to each other. On the other hand, complexes **3** and **4** show the single-channel relaxation of magnetization, and their isostructural character allowed to study the relaxation changes caused solely by the replacement of terminal halido ligands. Finally, a wet lithographic technique have been used to evaluate both the processability of the complexes in solution and the fabrication of microstructured films.

Introduction

Since their discovery in 1993,[1] single-molecule magnets (SMMs) attract considerable interest due to the possibility to store the magnetization within a single molecule. The slow relaxation of magnetization after the removal of the external magnetic field is a characteristic feature of SMMs which are also called single-ion magnets (SIMs) when formed by mononuclear transition-metal complexes. Furthermore, the

possibility to alter the magnetization projection by external magnetic field predetermines their application potential in data storage, quantum computing, and molecular spintronics.[2-4] This kind of magnetic bistability arises from the strong single-ion magnetic anisotropy controlled by the interplay of the ligand field and spin-orbit coupling. The magnetic anisotropy is the key parameter in the modulation of slow relaxation of magnetization and is proportional to the thermal energy barrier of the spin reversal U according to the equations $U = |D|(S^2 - 1/4)$ and $U = |D|S^2$ for Kramers and non-Kramers ions, respectively. While the research in the past was oriented on the systems with giant spin number S,[1,5,6] nowadays the interest is focused on the enhancement of axial magnetic anisotropy parameter D, in the complexes with the single metal center.[7-14] Indeed, the recent reports about the record-breaking blocking temperatures of SIMs[10-12] prove that mononuclear lanthanide complexes are considered as promising families which enable tuning of magnetic anisotropy by rational design of the ligand field strength and geometry of coordination environment.

Apart of the rare-earth element complexes, the Co(II) SIMs present another outstanding class of complexes due to the presence of strong first−order spin−orbit coupling, non-integer ground spin state (S = 3/2), and high magnetic anisotropy which is possible to control by the coordination number and symmetry of metal ion environment.[13-15] It is worth to mention, that the pentacoordinate Co(II) complexes with one rigid tridentate N-donor ligand (i.e. *terpy*) and two terminal ligand anions present an exciting family of the field-induced SIMs,[16-19] where the correlation between the geometry of coordination polyhedra and the magnetic anisotropy might help to understand the impact of the molecular design on relaxation dynamics. Some of us recently reported series of pentacoordinate Co(II) SIMs containing 2,6-bis(benzimidazole-1-yl)pyridine tridentate ligands, where the fine tuning of the geometry, anisotropy, and finally the parameters of slow relaxation of magnetization was possible to achieve by the variation of terminal halido or pseudohalido ligands.[19] Furthermore, the aromatic skeleton of employed tridentate ligands allows the introduction of miscellaneous substituents in order to enhance the further electronic (σ, π-donation/back-donation) and other physical properties (i.e. polarity, solubility in low polar solvents, thermal stability…) of desired pentacoordinate Co(II) SIMs.

Despite the demonstration of groundbreaking results in SMM research, the realization of interesting applications of such magnetically bistable molecular switches still remains a great challenge related to the attachment of the complex molecules onto the miscellaneous substrates.[19] In this regard, only a couple of successful studies about 3*d* transition metal complexes and even fewer reports about Co(II) mononuclear complexes were achieved while tuning and/or keeping the inherent magnetic properties of the SMM itself.[20,21] The crucial for this is to understand the anchoring and behavior of the SIMs molecules on the surfaces since their exposed surface offers many application possibilities but also brings many challenges, as these molecules can become redox unstable and decompose. There are two main routes how to produce the nanostructured magnetic surfaces – either by thermal sublimation of SIMs molecules in vacuum[21-23] or via wet-chemistry protocol from solutions.[24,25] Despite that the earlier approach allows precise surface functionalization in a well-defined and pure manner, it often demands

sufficient thermal stability and neutral SIMs molecules. On the other hand, the wet techniques are sufficient also for the charged SIMs and are usually limited only by the solubility of coordination compounds in the organic volatile solvents used for the surface deposition. Therefore, careful molecular design needs to be applied in the goal-directed synthesis of novel tailor-made SIMs for the surface characterization by lithography techniques. In particular, special attention must be paid to the allocation of substituents supporting the solubility of complex molecules in organic solvents (i.e. aliphatic alkyl substituents), in order to achieve sufficient thickness, quality, and pattern of surfaces.

Herein we report on the four mononuclear Co(II) complexes containing 2,6-bis(benzimidazole-1-yl)pyridine tridentate ligands functionalized with aliphatic n-octyl (L1) and n-dodecyl (L2) substituents and the next two coordination places are taken by chlorido or bromido terminal ligands (Scheme 1). The structural investigation confirmed expected molecular structures of **1**-**4** which can be expressed by the general formula $[Co(L1)X_2]$ or $[Co(L2)X_2]$ (where $X=Cl^-$ for **1**, **3** or Br^- for **2**, **4**; Scheme 1). All four compounds crystalize in monoclinic P-1 space group and further temperature variable structural study revealed reversible crystallographic phase transition in complex **2**, which has a notable impact on the static magnetic properties. The high-spin state magnetic behavior of **1**-**4** was analyzed by means of spin Hamiltonian as well as Griffith-Figgis Hamiltonian, and in combination with the *ab initio* calculations identified the triaxial anisotropy in the **1** and **2** and axial anisotropy in **3** and **4** of pentacoordinate Co(II) systems. Sensitivity of this class of complexes with respect to subtle setting of coordination environment was mirrored in the variations in their d-orbital ordering and consequent variations in static magnetic properties. The low-temperature EPR spectra of studied compounds were analyzed within a simplified effective spin-1/2 model for the description of the effective *g*-tensor components of the ground Kramers doublet. The anisotropy of the *g*-tensor agrees well with the predictions obtained within the CASSCF-NEVPT2 theory. FIRMS spectra did not provide enough resolution for determination of the precise *g*-tensor, therefore only g_{iso} was determined. Dynamic magnetic investigation revealed field-induced slow relaxation of magnetization in all four reported compounds. A curious case of two-channel relaxation was identified in the isostructural analogues **1** and **2** containing L1 ligand with octyl substituents. On the other hand, isostructural and isomorphous compounds **3** and **4** show single-channel relaxation, and their highly similar structural features allowed us to investigate the impact of the terminal halido ligand variation on the parameters of the magnetization relaxation. Wet processing of complexes using a lithographic technique has enabled the fabrication of microstructured films on technological substrates by exploiting their solubility. On the other hand attempts to deposit the repored complexes by sublimation failed due to the decomposition of complexes.

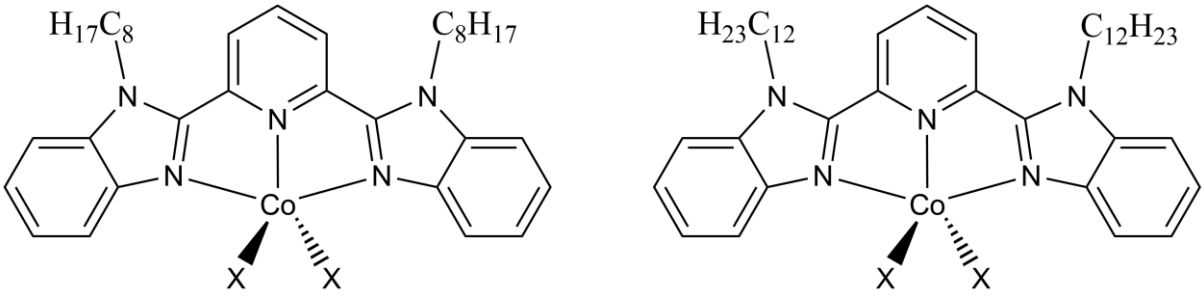

$[Co(L1)X_2]$

X= Cl^- for **1** and Br^- for **2**

$[Co(L2)X_2]$

X= Cl^- for **3** and Br^- for **4**

Scheme 1 Visualization of the molecular structures of reported compounds **1-4**.

Results and discussion

Syntheses and structural investigation

The synthetic procedures, characterization of reported compounds along with the technical details of the experimental and theoretical investigation are described in the supplementary information (SI). Tridentate ligands L1 and L2 were prepared by nucleofillic substitution between unsubstituted 2,6-bis(1*H*-benzimidazole-2-yl)pyridine and corresponding alkylhalogenide. While the synthesis of L2 bearing the dodecyl substituents afforded exclusive formation of desired product, the preparation of L1 was impeded by the formation of monosubstituted side-product $L1_m$ in low yield. Complexes **1-4** were prepared by the reaction of corresponding ligands with Co(II) salts and single crystals suitable for the diffraction analysis were isolated after few days of slow crystallization from acetonitrile solution. The phase purity of samples was confirmed by powder X-ray diffraction analysis prior to all physical properties investigation (Figure S14, see SI).

Single crystal diffraction studies confirmed the expected molecular structures of pentacoordinate Co(II) complexes **1-4**. All four compounds crystallize in triclinic P-1 space group and selected structural parameters are listed in Table S1 (see SI). The asymmetric unit of each solvent-free structure consists of one molecule of neutral complex expressed by the general formula **$[Co(L1)X_2]$** or **$[Co(L2)X_2]$** (X = Cl^- for **1** and **3**, Br^- for **2** and **4**, Figure 1) and two of them are included in the corresponding unit cell of **1-4**. In order to explain the anomalous step observed in the magnetic behavior of **2** (*vide infra*), the structural characterization was performed at two temperatures (100 and 200 K) and the careful comparison of both crystal structures along with the DCS measurement (Figure S15, see SI) revealed a reversible crystallographic phase transition at 167 K between two different triclinic P-1 low-temperature **2LT** (<167 K) and high-temperature **2HT** (>167K) polymorphs. This phase transition is associated mainly with the structural reorganization of alkyl chain positions causing significant changes in the unit cell parameters (Figure S16 and S17, see SI). Furthermore, a careful comparison of crystal structures of chlorido and bromido analogues revealed two isomorphic couples **1**-**2HT** and **3**-**4**.

The pentacoordinate Co(II) metal centers are surrounded by three nitrogen donor atoms of tridentate ligand **L1** or **L2**, and the next two coordination sites are occupied by two corresponding halido anions

X^- (Figure 1). Co-N distances vary in the range 2.09 - 2.15 Å and indicate the high-spin state of central atoms. Co-N3 bonds which involve pyridine nitrogen atoms are the shortest in coordination polyhedra of **1**, **3** and **4** (≈2.10 Å). However, this coordination bond is significantly prolongated in the low-temperature structure **2LT** (2.14 Å) and the phase transition causes its shortening down to 2.11 Å, as is detected at 200 K. In **1**-**4**, distances of Co-N bonds formed with imidazole nitrogen atoms (N1, N4) span from 2.12 to 2.15 Å and Co-X bonds formed with halido terminal ligands are the longest within the coordination polyhedra (d_{avg}(Co-Cl) = 2.31 Å; d_{avg}(Co-Br) = 2.46 Å). Addison τ_5 parameter expresses the degree of Berry pseudorotation between square pyramid (SPY) and trigonal bipyramidal (TBPY) shape of coordination polyhedra. In all reported structures, τ_5 varies in the range 0.08-0.13 suggesting the SPY shape of $\{CoN_3X_2\}$ coordination chromophores of **1**-**4**. Moreover, several ideal five-coordinate geometries were compared with polyhedra of **1**-**4** in more complex SHAPE structural analysis (Figure 1, Table S2, Figure S18). The lowest values of symmetry measure parameters are calculated for SPY shapes of coordination polyhedra (S(SPY)=2.1-2.6) and their possible deviations might lead towards TBPY and/or to vacant octahedral geometries (S(TBPY)=3.4-6.6; S(vOC)=4.1-4.9). The basal planes of SPYs are formed with three N donor atoms of the corresponding tridentate ligand and one halide anion. Co(II) central atom is pulled out from the basal plane (d(Co$\cdots${N1,N3, N4,X}$_{basal\ plane}$) in the range 0.47-0.55 Å) towards the apical axis of the pyramid, which is formed by the second X^- ligand.

It is worth noting that systems **3** and **4** have almost exactly the same spatial arrangement of all atoms in the crystal lattice (Figure S19) and minor differences between them are caused mainly by the prolongation of corresponding Co-X bond lengths (ca 0.14 Å) due to the presence of different halide in the structure (Table S2). In order to express the degree of similarity between the corresponding coordination polyhedra, we established a new parameter S calculated as a summation of differences between 10 corresponding angles of two pentacoordinate polyhedra (Figure S19). The comparison of **1** and **2LT**, **1** and **2HT,** or **2LT** and **2HT** resulted in values S=34.1°, 14.8° or 22.5°, respectively, indicating the significant differences in plasticity of corresponding polyhedra. On the other hand, the polyhedra of isostructural and isomorphic couple **3** and **4** acquire only small differences between the corresponding angles which is expressed by a low value of S=5.2°.

The detailed investigation of crystal structures of **1**-**4** revealed the presence of several weak intermolecular contacts formed between aromatic moieties of the neighboring molecules (Figure S20, see SI). Their lengths range just on the border of van der Waals radii summations of two C atoms (≈3.40 Å) and are responsible for the formation of head-to-tail pseudo-dimeric couples aligned within the *a*-*c* (**1** and **2LT**, **2HT**) or *b*-*c* (**3** and **4**) planes. The "in-dimer" Co···Co distances span from 6.72 Å to 7.41 Å, while Co···Co distances between neighboring dimer's complexes are in the range 8.38-8.71 Å.

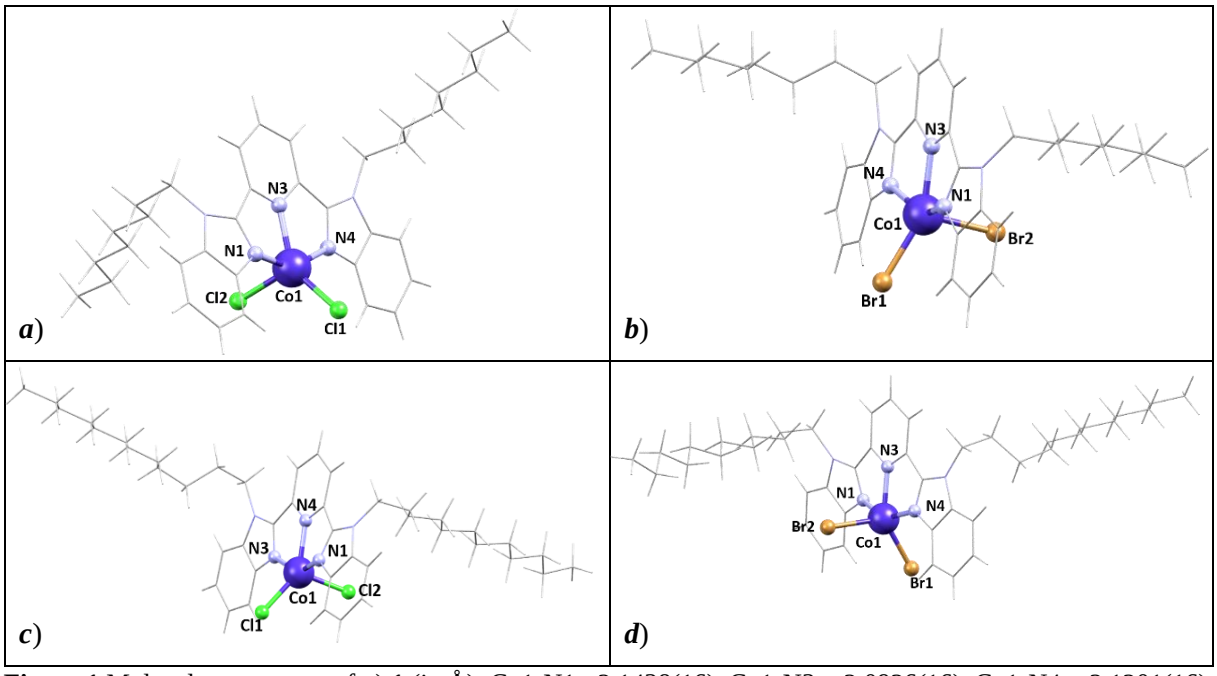

Figure 1 Molecular structures of ***a***) **1** (in Å): Co1-N1= 2.1438(16), Co1-N3 = 2.0926(16), Co1-N4 = 2.1201(16), Co1-Cl1 = 2.2911(5), Co1-Cl2 = 2.3112(5), τ_5=0.18, S(SPY)=2.403, S(TBPY)=3.457 , S(vOC)= 4.639; ***b***) **2LT** (in Å): Co1-N1 = 2.1115(16), Co1-N3 = 2.1372(15), Co1-N4 = 2.1102(16), Co1-Br1 = 2.4498(3), Co1-Br2 = 2.4674(4), τ_5=0.13, S(SPY)=2.122, S(TBPY)=6.649 , S(vOC)= 4.078; **2HT** (in Å): Co1-N1 = 2.129(2), Co1-N3 = 2.110(2), Co1-N4 = 2.111(2), Co1-Br1 = 2.4580(3), Co1-Br2 = 2.4387(4); τ_5=0.08, S(SPY)=2.435, S(TBPY)=4.697, S(vOC)= 4.756; ***c***) **3** (in Å): Co1-N1 = 2.1469(11), Co1-N3 = 2.1000(11), Co1-N4 = 2.1213(11), Co1-Cl1 = 2.2996(4), Co1-Cl2 = 2.3239(4), τ_5=0.12, S(SPY)=2.215, S(TBPY)=4.697, S(vOC)= 4.756; ***d***) **4** (in Å): Co1-N1 = 2.134(3), Co1-N3 = 2.097(3), Co1-N4 = 2.109(3), Co1-Br1 = 2.4411(6), Co1-Br2 = 2.4652(6), τ_5=0.08, S(SPY)=2.577, S(TBPY)=4.789, S(vOC)= 4.932.

Computational study and static magnetic properties

Although studies on static magnetism of pentacoordinate Co(II) complexes with pseudo-C_{4v} symmetry (i.e. approaching SPY or vOC shape of coordination environment) are not rare, there is not clear from the literature what is the conceptually correct approach to their static magnetism. As a matter of fact, the authors use almost exclusively the ZFS spin Hamiltonian (SH, *vide infra*) to analyze the experimental magnetization functions.[16,26-36] The main problem is, however, that its parameters bear a straightforward physical meaning only if the ground state is orbitally non-degenerate and well separated from closest excited states[37] and none of these assumptions need to be fulfilled in the mentioned class of systems. Another option is the Griffith-Figgis Hamiltonian (GFH, *vide infra*) which has been originally designed for octahedral systems possessing (or approaching) orbitally triple-degenerate ground state.[37] In contrast, pentacoordinate Co(II) complexes with pseudo-C_{4v} symmetry possess usually a non-degenerate or double-degenerate ground state, that can be modelled only as an extreme case within GFH model. The situation is also complicated by the fact, that the presence of degeneracy depends upon subtle geometry changes of the coordination environment. Indeed, a CASSCF-NEVPT2 calculation (*vide infra*) shows, that a simple model system $[Co(NH_3)_5]^{2+}$ possesses a double-degenerate ground state in SPY geometry and a non-degenerate ground state in vOC geometry while keeping perfect C_{4v}

symmetry of coordination environment in both cases (Figure S21, see SI). A simple DFT calculation reached the same conclusion in a previous work.[16]

These issues motivated us to gain some more insight into the electronic structure of studied complexes before starting with analysis of their magnetism. We thence defined five model molecules by cutting off the long aliphatic chains from experimental molecular geometries: **I** and **III** from chlorido-complexes **1** and **3**, respectively, and **II-LT**, **II-HT** and **IV** from low-temperature and high-temperature form of bromido-complex **2** and from bromido-complex **4**, respectively (Figure 4). In fact, within this set, the molecules with common halido-ligand possess identical formulas differing only in bond and angle distortions. For every model molecule a state-averaged CAS[7,5]SCF calculation was performed, that is, an optimal set of five molecular *d*-like orbitals (called *complete active space*, *CAS* hereafter) was sought, which can best describe all possible spin doublet and spin quartet states arising from seven electrons in these *d*-like orbitals (*CAS roots* hereafter). As a next step, the energy of every CAS root was corrected for interaction between seven electrons from within CAS and all other electrons in molecule using the method NEVPT2.[28] Finally, *ab-initio* Ligand-Field Theory[38] (*AILFT* hereafter) was employed, by which energy of all states is projected upon the effective ligand-field Hamiltonian. One-electron eigenstates of AILFT Hamiltonian resemble then the textbook atomic d-orbitals and their corresponding eigenvalues can be interpreted as information on the splitting of d-orbitals due to crystal-field. Some representative resulting AILFT orbitals with assigned symmetry labels of group C_{4v} are displayed in Figure S22 (see SI) and energy ordering of all orbitals is displayed in Figure 2a.

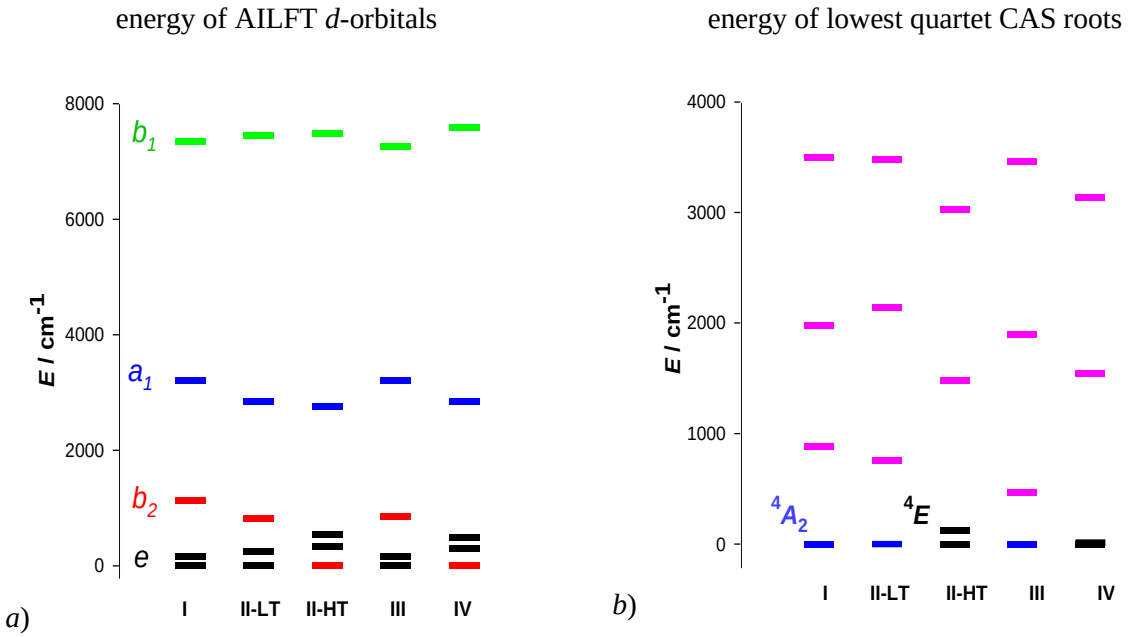

Figure 2 ***a***) Energy of AILFT *d*-orbitals in molecules **I-IV**, black: *e* orbitals, red: b_2 orbitals, blue: a_1 orbitals, green: b_1 orbitals; ***b***) energy of lowest lying quartet CAS roots in molecules **I-IV** calculated by CAS[7,5]SCF-NEVPT2 with assignment to crystal-field terms, blue: A_2 terms, black: *E* terms, pink: terms for which the symmetry label cannot be reliably assigned within C_{4v} point group.

One can see that in molecules **I**, **II-LT** and **III** a quasi-degeneracy of the two lowest orbitals is predicted in contrast with molecules **II-HT** and **IV**. By expressing the composition of CAS roots by means of AILFT orbitals (Table S3 and related comments, see SI) the low-lying crystal-field terms (*CFT* hereafter) can be identified. It turns out that **II-HT** and **IV** possess double-degenerate ground term ^4E (Figure 2b) while all other systems are orbitally non-degenerate in their ground state. There is also interesting to notice the difference in orbital degeneracy (and consequently in the ground CFT) associated with the slight changes of bond angles in coordination environment of **II-LT** and **II-HT**. In fact, comparison of their geometry shows, that **II-HT** is more "SPY-like" (Figure S18 and S19, see SI) so the relationship between geometry distortion and orbital ordering appears to bear the same features like in the case of $[Co(NH_3)_5]^{2+}$ (*vide supra*). Another striking fact is, that **III** and **IV** possess basically the same geometry, the only difference being the replacement of chlorido ligand (**III**) by bromido ligand (**IV**), however, their orbital ordering is different. Nevertheless, based on simple arguments of Atomic Overlap Model, it can be shown (see SI), that stronger π-donation ability of a ligand should destabilize the double degenerate orbitals within SQP geometry. As bromido ligand is stronger π-donor, it is exactly what was observed.

Straightforward application of the CFT assignment technique predicts orbital degeneracy for most of higher-lying CFTs (i.e. *E* terms), which however does not appear to be the case when looking at considerable energetic gaps between the higher lying CAS roots (pink color in Figure 2b). Such discrepancy can be attributed to non-ideal geometry of the coordination environment of model molecules. Indeed, by symmetry transition from C_{4v} to D_{3h} in pentacoordinate Co(II) systems, the induced splitting of degenerate terms is expected to be more pronounced for the excited ones.[40]

Based on this discussion there is clear, that none of the two above mentioned models is expected to be universally applicable in the studied class of molecules, nevertheless, we tested the performance of both. The SH was defined in the form

$$\hat{H}_{SH} = D\hat{S}_z^2 + E\left(\hat{S}_x^2 - \hat{S}_y^2\right) + \mu_B \vec{\hat{S}} \cdot \overline{\overline{g}} \cdot \vec{B} \qquad (1)$$

where *D* and *E* are axial and rhombic parameters of zero-field splitting, respectively, $\vec{B}$ is the vector of magnetic field induction, $\overline{\overline{g}}$ is the gyromagnetic tensor and $\vec{\hat{S}}$ and $\hat{S}_{x,y,z}$ are the vector operators of spin and its components, respectively.[41] The Griffith-Figgis Hamiltonian was postulated in the following form

$$\hat{H}_{GFH} = -\frac{3}{2}\lambda \vec{\hat{L}} \cdot \vec{\hat{S}} + \Delta_{ax}\hat{L}_z^2 + \Delta_{rh}\left(\hat{L}_x^2 - \hat{L}_y^2\right) + \left(-\frac{3}{2}\vec{\hat{L}} + 2\vec{\hat{S}}\right) \cdot \vec{B} \qquad (2)$$

where $\vec{\hat{L}}$ and $\hat{L}_{x,y,z}$ are vector operators of angular momentum and its components, respectively, λ is the constant of spin-orbit interaction and Δ_{ax} and Δ_{rh} are parameters of crystal field of axial and rhombic symmetry, respectively.[37] To improve the agreement between models and experiment, the effect of

molecular field was included in both cases (quantified by parameter *zj*), which accounts for weak magnetic exchange interaction with neighbouring magnetic centres.

Magnetic characterization of compounds **1-4** was examined in the temperature range 2-300 K at B_{DC}=0.1 T and in the field range B_{DC}=0-7 T at two temperatures 2 K and 4.6 K. Both measurements are represented in Figure 3 as χT vs T and M_{mol} vs B functions. The room temperature values of χT (2.95-3.21 $cm^3\ mol^{-1}\ K^{-1}$) are significantly higher than the spin-only value for S=3/2 system (1.876 $cm^3\ mol^{-1}\ K^{-1}$) suggesting considerable contribution of angular momentum. On lowering the temperature, the χT product of **1** and **4** obey Curie law up to ca 100 K and then gradually decrease reaching 2.5 and 2.3 $cm^3\ mol^{-1}\ K^{-1}$ at 2 K, respectively. On the other hand, χT product of **3** slowly increases upon the cooling, reaches a maximum of 3.76 $cm^3\ mol^{-1}\ K^{-1}$ at 82 K and gradually decreases down to 3.3 $cm^3\ mol^{-1}\ K^{-1}$ at 2 K. Interestingly, χT vs T curve of **2** reflects the crystallographic phase transition bellow 167 K (*vide supra*) which occurs as the sharp step from 2.97 $cm^3\ mol^{-1}\ K^{-1}$ to 2.81 $cm^3\ mol^{-1}\ K^{-1}$. This is in agreement with expectation, since the magnetic moment of *E*-terms in contrast with that of *A*-terms can be increased by orbital angular momentum.[39,42] Further cooling of **2LT** causes gradual lowering of χT down to 1.9 $cm^3\ mol^{-1}\ K^{-1}$ at 2 K. Measurement in the heating and in the cooling proved the reversibility of the transition between **2LT** and **2HT** phases which is accompanied by small hysteresis loop ($\Delta T \approx 4$ K, Figure 3b inset). Molar magnetization M_{mol} at 7 T and 2 K acquires lower values (2.32-2.63 μ_B) than expected for a Curie paramagnet with S=3/2 (3 μ_B), which indicates notable magnetic anisotropy. The temperature dependence of χT and field function of magnetization were fitted simultaneously for every compound except **2HT** due to very limited data available. The optimum parameter values are collected in Table 2 and experimental functions along with their optimum fits are displayed in Figure 3 for SH model and in Figure S23 for GFH model. As apparent from the values of combined error residuals $R(\chi T)*R(M)$ and from visual comparison, SH performs in general much better than GFH in this set of compunds. Moreover, it eventually turned out as unnecessary to include the rhombic ZFS parameter for obtaining satisfying fits and it was therefore omitted.

Table 1. Optimum fit values of parameters of spin Hamiltonian and Griffith-Figgis Hamiltonian

	1	**2LT**	**3**	**4**
parameters from optimum fit of experiment to SH				
D (cm^{-1})	-69(1)	-42.9(4)	-78(2)	-66(1)
g_1	2.21(5)	2.25(1)	1.92(2)	2.24(1)
g_2	2.42(2)	2.498(9)	2.16(1)	2.476(9)
g_3	2.96(1)	2.608(1)	3.280(3)	2.89(2)
zj (cm^{-1})	0.0006(2)	-0.001(1)	-0.006(1)	-0.0006(8)
$R(\chi T)*R(M)$	0.022	0.028	0.041	0.003
parameters from optimum fit of experiment to GFH				
λ (cm^{-1})	-165.9	-178.0	-172.4	-160.1
Δ_{ax} (cm^{-1})	-3153	-328.7	-1952	-2378
Δ_{rh} (cm^{-1})	-8(4)	-99.2	0.0	-82(2)
zj (cm^{-1})	-0.0006(1)	-0.047	-0.039	+0.006(7)
$R(\chi T)*R(M)$	8.5	0.205	313.7	0.444

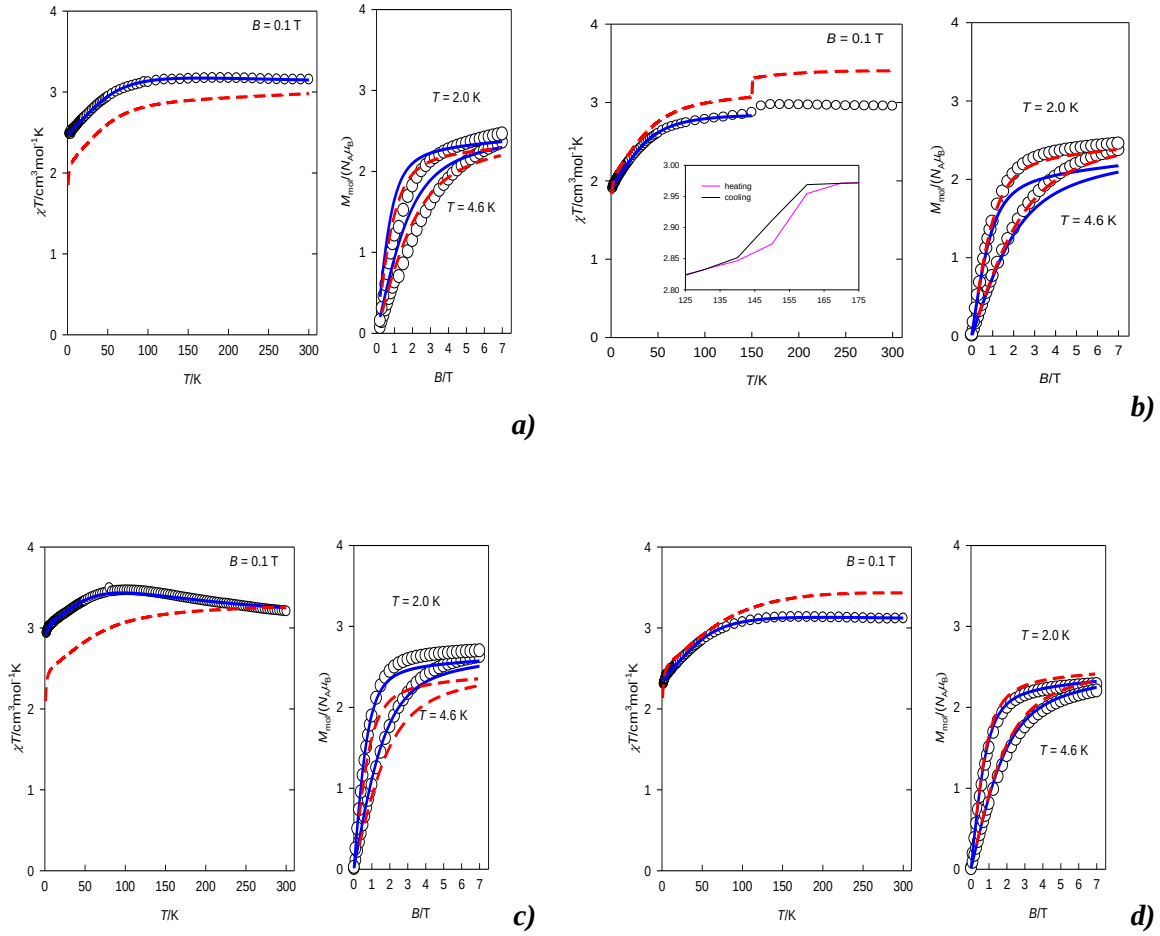

Figure 3 Magnetic functions analyzed by Spin Hamiltonian for ***a***) compound **1**; ***b***) compound **2**; ***c***) compound **3** and ***d***) compound **4**. Left: susceptibility-temperature product with respect to temperature, right: magnetization per center with respect to the magnetic field; empty circles: experiment, blue solid line: optimum fit, red dashed line: *ab-initio* prediction based on model molecules.

Having determined the SH as acceptable effective model for interpretation of magnetism in **1**-**4**, its optimum parameter values can be confronted with those predicted by CASSCF-NEVPT2 wavefunctions of **I**-**IV**. For this sake the spin-orbit interaction (SOI hereafter) between individual magnetic eigenstates must be included to this approach which reveals finer structure of energy eigenstates. More specifically, the splitting of CAS roots to the Kramers' doublets becomes apparent and from their structure the SH parameters can be extracted (see also Table S4 in SI). Two strategies for such parameter extraction are common: the effective Hamiltonian method and perturbation theory. Both were used here and the obtained values are collected in Table 2. As a rule of thumb, the computed values of ZFS parameters are considered reliable if these two approaches meet in their predictions. Such condition is fulfilled only for **I** and less so for **II-LT**. This supports the argument that spin Hamiltonian is not well defined if the ground state is orbitally degenerate or nearly-degenerate. Nevertheless, the agreement between the magnitude of fitted values (SH approach without rhombicity, Table 1) and predicted values (SH

parameters extracted by effective Hamiltonian method from CASSCF-NEVPT2 wavefunciton of model molecules, Table 2) is satisfactory for all systems.

Table 2 Calculated values of parameters of spin Hamiltonian and Griffith-Figgis Hamiltonian

	I	**II-LT**	**II-HT**	**III**	**IV**
SH parameters from effective Hamiltonian for the ground term by CAS[7,5]SCF/NEVPT2					
D (cm^{-1})	-61.65	48.77	-98.11	-91.41	-98.56
E/D	0.264	0.251	0.237	0.162	0.197
g_x	2.00	2.80	1.29	1.95	1.52
g_y	2.30	2.51	1.55	2.14	2.03
g_z	2.81	2.04	3.19	3.06	3.20
SH parameters from second-order perturbation theory for the ground term by CAS[7,5]SCF/NEVPT2					
D (cm^{-1})	-76.95	64.94	-481.8	-150.79	-4599.3
E/D	0.255	0.277	0.039	0.118	0.008
spin-orbit coupling parameter by CAS[7,5]SCF/NEVPT2/AILFT					
λ (cm^{-1})	-170.8	-168.1	-168.1	-170.9	-168.1

Noteworthy, the sign of computed D parameter of **II-LT** is opposite of all other. Such discrepancy can be considered a calculation artifact, since when the value of ratio E/D approaches 1/3 the sign of ZFS parameters is meaningless and rather than easy-axis or easy-plane anisotropy, the *triaxial anisotropy* should be attributed to the system.[36]

Regarding the contrast between the limitations of SH and GFH models and the factual reality of magnetic anisotropy, there appears a natural question whether an alternative way of anisotropy assessment can be found, providing that a relevant wavefunction is available. Very recently a method combining measurement of experimental electron density and *ab-initio* calculations was described for special four-coordinated Co(II) systems.[43] Another strategy was introduced a few years ago where eiegenvalues of CASSCF-NEVPT2+SOI Hamiltonian perturbed by effect of magnetic field are evaluated for all directions with respect to the molecular frame.[44] Molecular magnetization as a response to acting magnetic field illustrates then the orientational preference of the molecular magnetic moment and the anisotropy is assessed visually. Herein we adopted the latter approach. For **I**-**IV** the SOI between all NEVPT2-corrected CAS roots (10 spin quartets and 40 spin doublets, i.e. 120 magnetic states) were evaluated. The resulting molecular magnetizations are displayed in Figure 4. Visual comparison suggests that all studied systems show qualitatively the same kind of axial-like anisotropy, having also similar orientation with respect to the molecular skeleton. To provide a reference, the intramolecular magnetic interaction was described also exclusively by SH inserting the parameter values from Table 2 (Figure S24, see SI). Comparison between these two sets of pictures shows a profound similarity and confirms what was indicated above: despite SH need not bear a straightforward physical interpretation in pentacoordinated Co(II) systems, it appears as a useful and well-performing effective model which is feasible to grasp the features of their magnetic anisotropy.

Finally, by spatial averaging of the molecular magnetizations the temperature and field dependent magnetic functions were created and displayed in Figure 3 and Figure S23 along with experimental and

fit curves. In fact, such functions are based purely on the *ab-initio* method and do not include any empirical parameters. Satisfying agreement with experiment can be concluded in all cases.

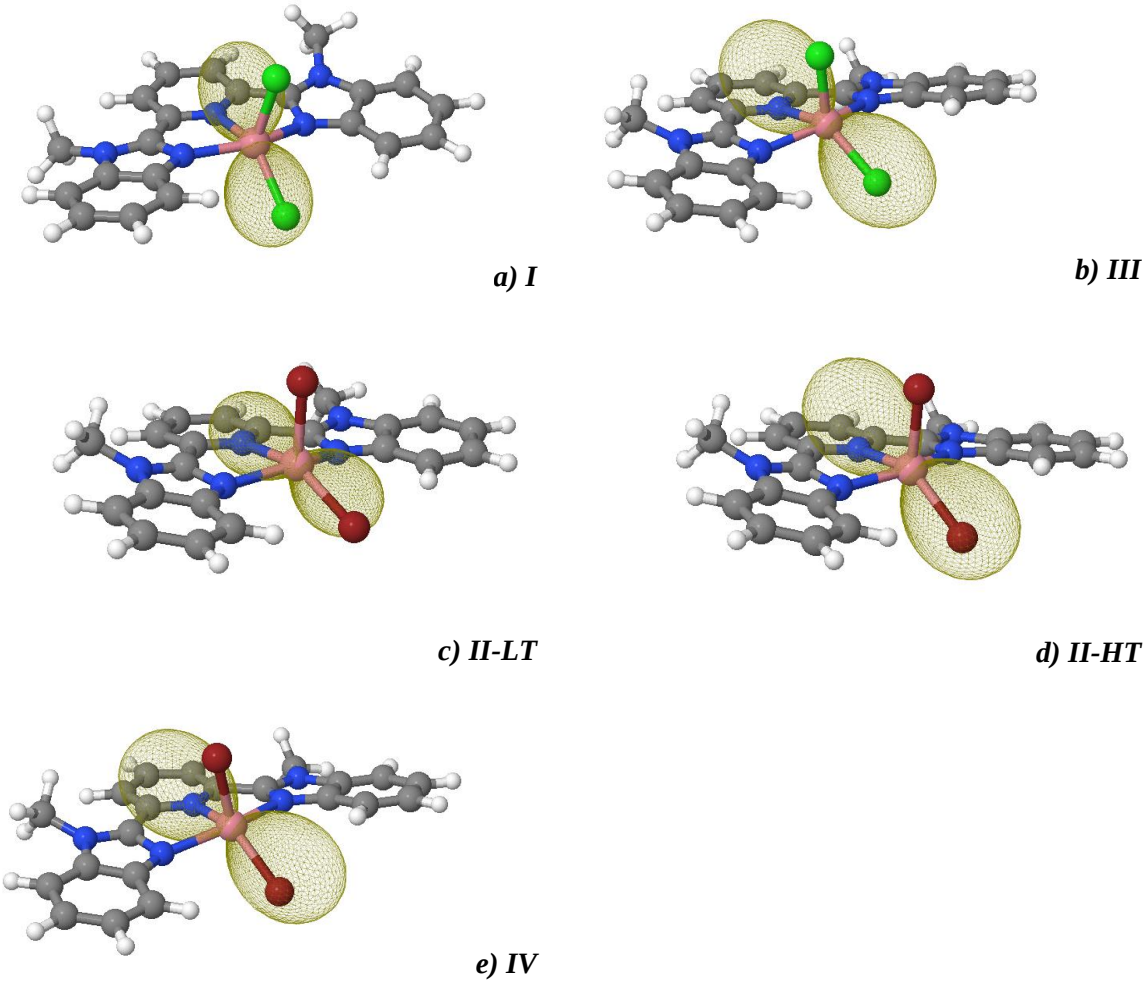

Figure 4 Orientational dependence of molecular magnetization with respect to the molecular frame for: ***a***) molecule **I**; ***b***) molecule **III**; ***c***) molecule **II-LT**, ***d***) molecule **II-HT** and ***e)*** molecule **IV**.

EPR study

The X-band EPR spectra of compounds **1-4** were measured in the temperature range from 2 K up to 40 K. The temperature evolution of the EPR spectra (Figure S25, see SI) shows a typical decrease of the signal intensity with increasing temperature for Co(II) complexes with a large energy gap between the ground and first-excited Kramers doublet as predicted by CAS[7,5]SCF-NEVPT2 calculations summarized in Table S5. Some non-trivial change of the spectra was observed at the lowest temperatures for compound **3,** but it can also be attributed to the evolution of anisotropic line broadening. A simplified effective spin-1/2 model describing only the ground Kramers doublet due to the strong splitting between the ground and excited Kramers doublets was used for the analysis. This model assumes the mixing of higher excited states with the ground-state Kramers doublet as the consequence of the spin-orbit coupling yielding highly anisotropic effective *g*-factors that reflect also the magnetization anisotropy. The simulation of EPR spectra was performed within the EasySpin simulation package.[45] The spectra

of compounds **3** and **4** also reveal partially resolved hyperfine coupling; therefore, it was included in the simulations. An anisotropic convolutional broadening ΔB (full-width at half-height) necessary to fairly reproduce the experimental data. For compounds **3** and **4,** the simulations in Figure 5 are intentionally shown with a reduced broadening of some spectra components to show the estimation of the components of the anisotropic hyperfine coupling parameter *A*. The values of the parameters obtained using the effective spin-1/2 model are summarized in Table 3. One may start the analysis of the obtained results using simplified geometries, like D_{4h}, effective *g*-factors directly allow revealing the type of the magnetic anisotropy (easy-axis or easy-plane) when compared with their theoretical prediction using GFH formalism. Within the GFH formalism (with axial Δ_{ax} and rhombic Δ_{rh} crystal field term included), one of the calculated effective *g*-factors components can reach high values $g > 6$, which can be assigned as g_z, and the other two, g_x and g_y, may fall well below 2 for the easy-axis anisotropy, which seems to be the case of the compounds **3** and **4**. On the other hand, the LT phase of compound **2** can be described by the effective *g*-factors $g > 2$ that would be compatible with the easy-plane anisotropy but with a relatively high rhombicity. At last, the EPR spectra of compound **1** show very strong line broadening, making it difficult to extract components of the *g*-tensor straightforward. The best agreement was again obtained for at least one component $g < 2$, the three distinct values of *g*-factor also suggest a significant rhombicity as in compound **2**. Such a result seems to be compatible with results obtained within the effective spin Hamiltonian approach in CAS[7,5]SCF-NEVPT2. But, it may not reflect the deviation from D_{4h} symmetry in the case of the studied compounds. For vacant octahedron in C_{4v} symmetry, the energies of one-electron *d*-orbitals have much smaller energy differences; the same is expected for CFTs. Thus the influence of excited states through the second-order SOC on the effective *g*-factors of the ground Kramers doublet is stronger, yielding more extreme values as for D_{4h} symmetry. Still, such prediction may not capture the experimental *g*-factors for a strong shift of the central ion from the square base towards the apical ligand as in studied compounds. We have also compared the results of the Angular Overlap model[46] for square pyramidal coordination of Co(II) ions, and the theory indeed predicts one very high *g*-factor component $g > 6$. Interestingly, the hyperfine coupling parameter *A* corresponding to the largest *g*-factor component is predicted to reach very high values as observed in the experimental EPR spectra of studied compounds. But the assignment of *x,y,z* coordinates for *g*-factor components may not be as straightforward as in the case of GFH formalism for D_{4h}. Angular Overlap model predicts the extreme value of $g>6$ for C_{4v} as g_z in the case of $CoAB_4$ chromophores and as g_y for CoA_5 chromophores. It should be noted that the spin-Hamiltonian formalism does not allow us to estimate the value of the *D* parameter for large values as predicted for compounds **1**-**4** (only *E*/*D* ratio eventually) from X-band EPR. In summary, the overall anisotropy of the estimated *g*-factor components from EPR spectra agrees with the CAS[7,5]SCF-NEVPT2 calculations. However, experimental values of the lowest *g*-factors do not reach the extreme theoretical predictions reported in Table S5 on model structures.

Table 3 Parameters describing the low-temperature X-band EPR spectra of compounds **1**-**4** using an effective spin-1/2 model including the hyperfine coupling.

	1	**2LT**	**3**	**4**
g_1, g_2, g_3	1.69, 3.90, 6.0	2.10, 3.40, 8.0	1.33, 1.66, 8.6	1.47, 2.12, 8.7
A_1, A_2, A_3 (MHz)	420, 340, 1600	320, 435, 1100	60, 500, 1650	250, 360, 1750
ΔB_1, ΔB_2, ΔB_3 (mT)	55, 70, 260	30, 35, 120	25, 25, 135	27, 50, 65

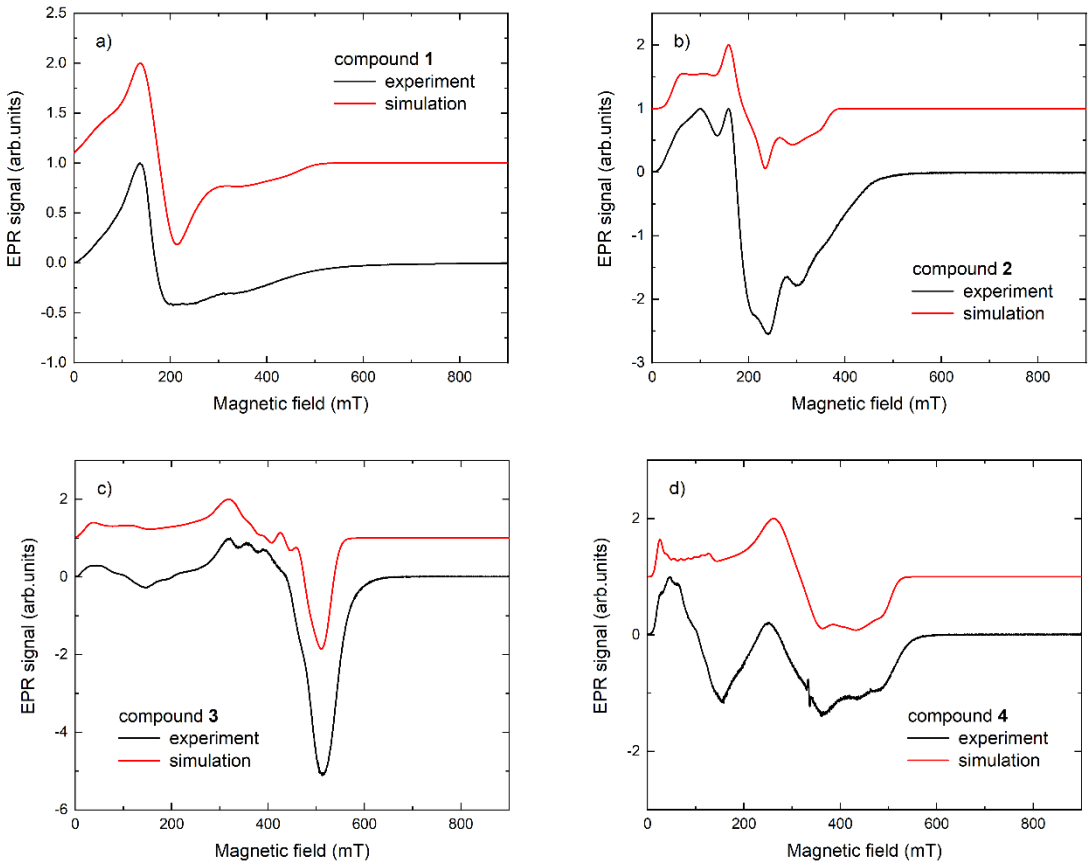

Figure 5 EPR spectra of ***a***) compound **1**; ***b***) compound **2**; ***c***) compound **3**, and ***d***) compound **4** measured at 9.4 GHz at 5 K (black lines). The simulation using the effective spin-½ model is shown by the red line above the experimental data.

Far Infrared Magnetic Spectroscopy

For a definitive determination of the zero-field splitting (ZFS), Far Infrared Magnetic Spectroscopy (FIRMS) was exploited. FIRMS enable us to observe EPR transitions of SMMs with large zero-field splitting, mainly based on transition metal complexes (SIMs), and determine ZFS directly from the spectra. For cobalt(II) complexes with S = 3/2, the zero-field splitting between two Kramers doublets is equal to $2(D^2 + 3E^2)^{1/2}$ (or $2D$ when omitting E). This energy gap is then directly observable in FIRMS spectra.

The FIRMS spectra were recorded on pressed powder pellets of **1**-**4** (diluted in eicosane) at T = 4.2 K, and magnetic fields up to 16 T. The spectra were normalized by the zero-field transmission spectra, T(0), and their corresponding reference transmission spectra, R(0). Normalized transmission spectra (Figure S26, S28, S30, S32) were then depicted in the form of a color map for better identification of the EPR transitions (Figure 6 and Figure S27, S29, S31, S33). In the color maps, the

tendency toward the yellow color means the absorbance increases, whereas the blue color corresponds to the transparent regions. All observed EPR transition were identified in the range of 50 – 300 cm^{-1}. Multiple field-dependent peaks can be found in this range, therefore the combination of theoretical calculations and magnetization experiments supported the choice of the peaks corresponding to the ZFS transition. FIRMS simulations, shown in dotted lines (Figure 6, S29, S31, S33) were calculated by means of the EasySpin Toolbox for Matlab[45] based on the SH and the parameters obtained from CASSCF-NEVPT2 calculations. Red color represents the strongly allowed transitions; grey color indicates forbidden/weakly allowed transitions.

In the normalized FIRMS transmission spectra (Figure S26) and the corresponding color map (Figure S27) of complex **1**, no EPR transition was observed (that could be related to a thicker sample or low dilution). Therefore, no simulation was used in this case. A color map of normalized FIRMS transmission spectra of complex **2** (Figure 6a) shows a clear field-dependence of one of the peaks, occurring at ~ 103 cm^{-1} at zero magnetic field and attributed to the EPR transition among $m_s = \pm 3/2$ to $m_s = \pm 1/2$ states. Based on the simulation and assuming $E/D = 0.251$ from the CASSCF-NEVPT2 calculations, the obtained ZFS parameter D for complex **2** is $D = -47\ cm^{-1}$ for $g_{iso} = 2.1$, which is in excellent agreement with the value in Table 1 and Table 2 obtained from magnetization experiments and theoretical calculations.

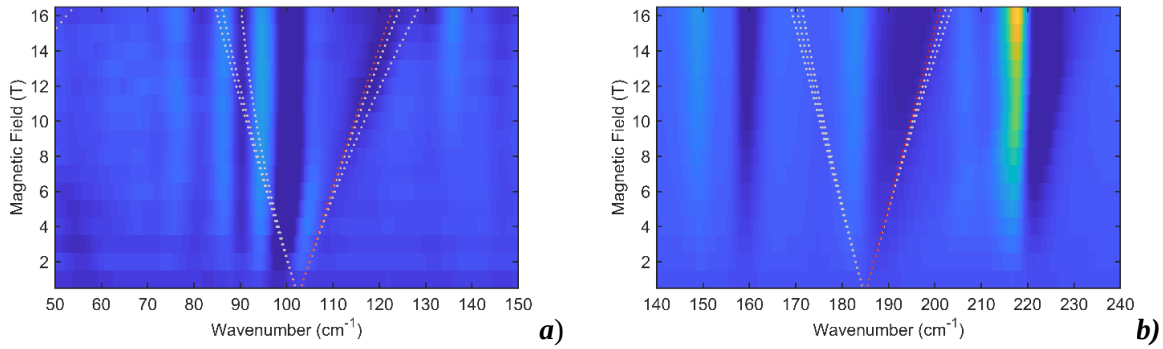

Figure 6 A color map of normalized FIRMS transmission spectra recorded on pressed powder pellet of ***a***) complex **2** and ***b***) complex **3**, both measured at T = 4.2 K and magnetic field up to 16 T. Spectra were normalized by zero-field transmission spectra division and corresponding reference transmission spectra division. Simulation with the SH ($S = 3/2$, $D = -47\ cm^{-1}$, $E/D = 0.251$, $g_{iso} = 2.5$ for **2** and $S = 3/2$, $D = -89\ cm^{-1}$, $E/D = 0.162$, $g_{iso} = 2.1$ for **3**) is shown as dotted lines. Red color represents the strongly allowed transitions; grey color indicates forbidden/weakly allowed transitions. The tendency toward the yellow color means the absorbance increases, whereas the blue color corresponds to the transparent regions.

The same approach was applied to the complex **3**, assuming $E/D = 0.162$, $g_{iso} = 2.1$, simulation based on CASSCF-NEVPT2 calculated parameters fits well the experimental FIRMS spectra (Figure 6b) and gives us $D = -89\ cm^{-1}$. This result is again in accordance with the D value in the Table 1 and Table 2. Similarly, in FIRMS spectra of complex **4**, based on simulation with $E/D = 0.197$, $g_{iso} = 2.7$, parameter $D = -89\ cm^{-1}$, and simulation fits well the experimental FIRMS spectra (Figure S33). The FIRMS result is in very good agreement with the D value from theoretical calculations and magnetization experiments.

In addition, spectra were normalized by dividing a transmission spectrum measured at B_0 by a spectrum measured at B_0 + 1 T[47] and depicted as a color map.[47] This approach enable us to observe less intense features in the color maps. Further details can be found in ESI Figures S34, S35, S36, S37.

Dynamic magnetic investigation

In order to probe the SIM behavior in **1**-**4**, temperature and frequency dependence of the alternating-current (AC) susceptibility was measured at low temperatures (see SI for a detailed experimental description of AC susceptibility measurements and data analysis). At 2 K, DC field scan for four frequencies of AC susceptibility revealed no out-of-phase signal χ'' at B_{DC}= 0 T (Figure S38, see SI), which is a consequence of fast relaxation of magnetization resulted from quantum tunneling effect induced by hyperfine interactions with the nuclear spins. However, the applied DC field caused the suppression of the tunneling effect, and the different evolution of χ'' for four selected frequencies of AC field suggests that **1**-**4** show the field-induced slow relaxation of magnetization. Further temperature and frequency-dependent dynamic studies were recorded at B_{DC}=0.1 T since all four compounds show the highest out-of-phase signal at that static field.

Compounds **1** and **2LT** exhibit frequency-dependent out-of-phase signal χ'' which was not possible to fit by one-set Debye model satisfactorily (equations S1 and S2, see SI). Despite that out-of-phase signals and Cole-Cole diagrams (Figure 7a, Figure S39, and S40) remind the single-channel relaxation, the fitting of both components of AC susceptibility for **1** and **2LT** was successful only after the employment of the two-set Debye model (equations S3 and S4). This analysis revealed a peculiar situation where the low-frequency (LF) and high-frequency (HF) relaxation channels are unusually close to each other (Table S7 and S8, Figure S39ef and 40ef). Relaxation times of both channels reach 25.92 ms (τ_{LF}) and 3.21 ms (τ_{HF}) for **1** and 1.77 ms (τ_{LF}) and 0.25 ms (τ_{HF}) for **2** at 1.9 K and temperature increase causes their dramatic lowering. In both compounds, the LF channels have a narrow distribution of relaxation times α_{LF} (5×10^{-3} - 0.1 for **1** and $\approx10^{-16}$ for **2**) which is however non-negligible in the HF channels (α_{HF} = 0.11-0.44 for **1** and α_{HF} = 0.15- 0.47 for **2**). At 1.9 K, the ratio of LF and HF branches are 40:60 for **1** and 30:70 for **2**, and temperature increase causes the complete vanishing of HF channel in favor of LF-one in **1** and balanced contribution of both LF and HF channels to overall relaxation the in the second complex (Figure S39h and S40h). Temperature dependence of relaxation times was analyzed in the sense of the equation

$$\frac{1}{\tau} = \frac{1}{\tau_0} exp\left(-\frac{U}{k_B T}\right) + CT^n + AB^m T \qquad (3)$$

where the corresponding terms describe thermally activated Orbach, Raman, and direct relaxation of magnetization, respectively. The most reliable fits of ln τ vs T^{-1} dependencies were reached for the combination of Orbach+direct (OD) or Raman+direct (RD) processes (Table S11 and S12, Figure 7cd), which allow comparison of the relaxation features in both compounds. The first OD approach for LF channels of **1** and **2** afforded similar values of U and τ_0 (U/K = 30.4(5) and 24.9(9), τ_0/s= $2.8(3)\times10^{-7}$

and 3.4(7)×10^{-7} for **1** and **2**, respectively), while the slope of direct process elevates upon the chlorido for bromido replacement (AB^m/T^{-m}K^{-1}s^{-1}=23.1(11) and 330(11) for **1** and **2**, respectively). Also in the case of RD analysis of LF channels of **1** and **2**, the preexponential factors *C* and exponents *n* are very similar (C/K^{-n}s^{-1}=8.3(12)×10^{-2} and 0.9(1), n=7.1(1) and 6.3(1) for **1** and **2**, respectively) and obtained values of AB^m for the direct process are in good agreement with those obtained from the OD fits (AB^m/T^{-m}K^{-1}s^{-1}=14.3(12) and 282(74) for **1** and **2**, respectively). The trend of increasing AB^m slope of the direct process upon the replacement of chlorido for bromido terminal ligands is also obvious in the HF channels. Both OD and RD fits indicate the notably higher AB^m constants in complex **2**, while the parameters of Orbach and Raman processes are more-or-less comparable with those observed for LF channels.

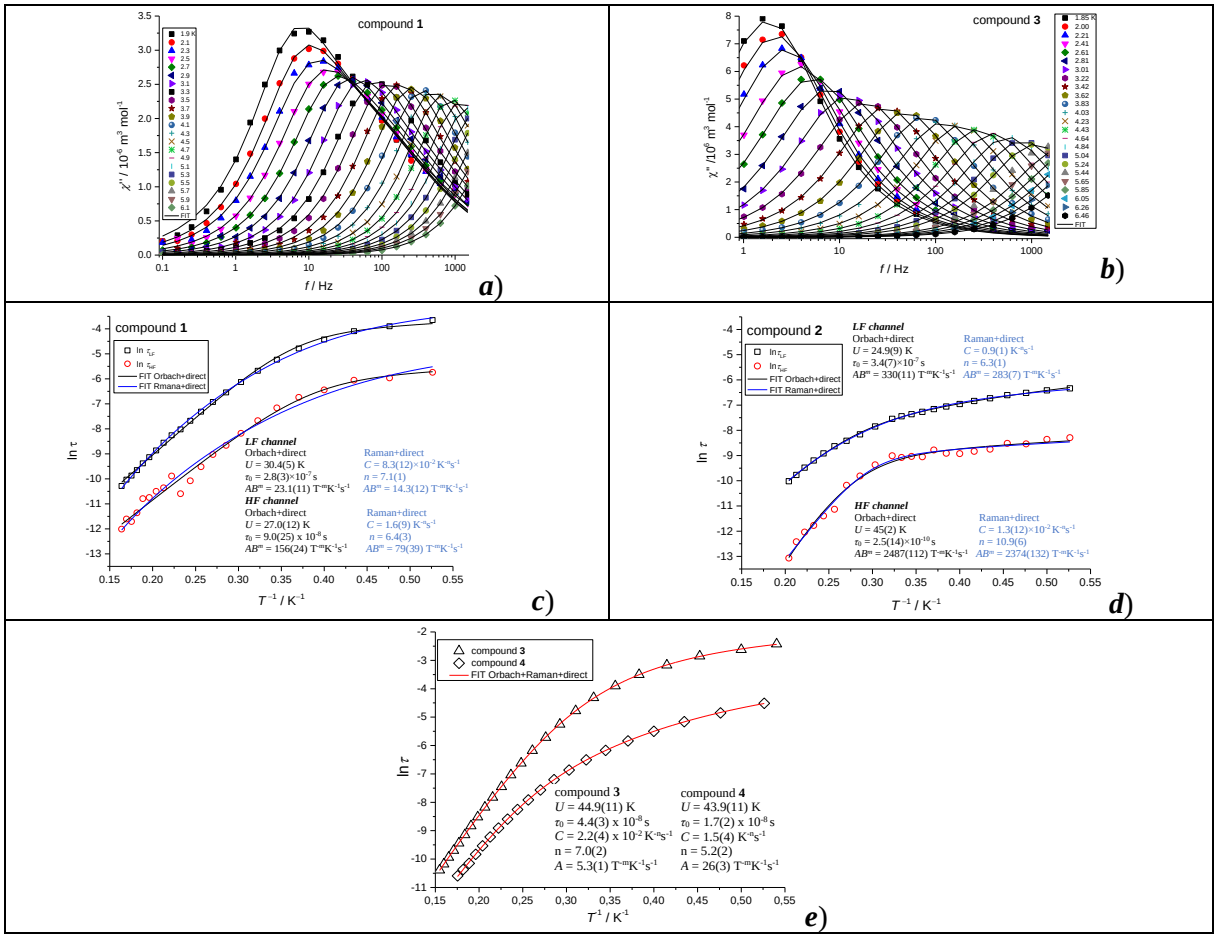

Figure 7 Frequency dependence of out-of-phase AC susceptibility for compounds **1** (***a***) and **3** (***b***). The solid lines are results of fits according to equations S3 and S4 (case of **1**) and S1 and S2 (case of **3**). ln τ vs T^{-1} dependencies for LF and HF relaxation channels of compounds ***c***) **1** and ***d***) **2**. ***e***) ln τ vs T^{-1} dependencies for compounds **3** and **4**.

On the contrary, the isostructural and isomorphic complexes **3** and **4** exhibit the single relaxation channel with clear frequency-dependent out-of-phase signal χ'' having the longest relaxation time τ=89 ms (for **3**) and τ=11 ms (for **4**) at 1.9 K (Figure 7b, Table S9 and S10, Figures S41 and 42). Thus, both compounds are field-induced SIMs and the fitting of AC susceptibility to the extended one-set Debye model (equations S1 and S2) allowed to analyze temperature evolution of τ in the sense of relaxation equation (3). At first, the single Orbach and single Raman fits were tested in the higher temperature

regions of the relaxation (>3.22 K for **3** and >3.5 K for **4**, Table S13 and S14). This resulted in the comparable height of energy barrier U and relaxation time at infinite temperature τ_0 for both complexes (U = 37.0(7) K and 31.3(8) K, τ_0/s=1.19(1)×10^{-7} and 1.16(2)×10^{-7} for **3** and **4**, respectively), while preexponential factor C of the Raman mechanism increases from the chlorido to bromido complex (C/K^{-n}s^{-1}=8.30(3)×10^{-3} and 0.184(7), n=8.20(6) and 7.07(6) for **3** and **4**, respectively). The more complex fits involving any combination of two or all three relaxation processes resulted in comparable values of fitted parameters with similar statistics of regression analysis (Table S13 and S14). Therefore, in order to effectively compare the relaxation parameters of both isostructural complexes, the following discussion is focused on the results obtained from fits involving all three Orbach, Raman, and direct mechanisms of relaxation. This approach shows again the highly comparable values of Orbach parameters for both isostructural compounds (U = 44.9(2) K and 43.9(11) K, τ_0/s= 4.4(1)×10^{-8} and 1.7(2) × 10^{-8} for **3** and **4**, respectively) and more pronounced preexponential factors of Raman and direct processes (AB^m) for bromido complex **4** (C/K^{-n}s^{-1}=0.022(4) and 1.5(4), n=7.0(2) and 5.2(2), AB^m/T^{-m}K^{-1}s^{-1}=5.3(1) and 26(3) for **3** and **4**, respectively). The Raman exponents are lower than the expected value of 9 for Kramers ions,[48] but when optical and acoustic phonons are considered, n in the range of 1 – 6 is reasonable.[49] Keeping in the mind high similarity of the molecular and crystal structures of **3** and **4**, the parameters obtained from the analysis of lnτ vs T^{-1} lead to a tentative conclusion that replacement of terminal halido ligand in pentacoordinated Co(II) SIMs can affect only the Raman and direct processes of relaxation. On the other hand, almost the same parameters of Orbach relaxation for **3** and **4** suggest that this process cannot be affected by the alternation of halido ligands while the other molecular and supramolecular features of isostructural analogues maintain the same. We tried to confirm this hypothesis by the comparison of herein reported Co(II) SIMs with the previously reported similar isostructural systems [Co(bbp)X$_2$]·MeOH,[17] [Co(bbp)X$_2$]·DMF,[49] [Co(tBuBzbbp)X$_2$][19] and cubic polymorphs of [Co(L)X]X[50] which contain halido terminal ligands X = Cl$^-$ or Br$^-$ (where bbp=2,6-bis(benzimidazole-1-yl)pyridine, tBuBzbbp=2,6-Bis(1-(3,5-di-tert-butylbenzyl)-1*H*-benzimidazol-2-yl)pyridine and L=tris(2-pyridylmethyl)amine). Table S15 presents an overview of the ZFS and relaxation parameters obtained at the same (or similar) experimental conditions (T, B_{DC}). The similar increase of C and AB^m pre-exponential factors caused by Cl$^-$ and Br$^-$ ligand variation observed in the isostructural couples **1-2LT** and **3-4** was found only for the cubic polymorphs of [Co(L)X]X complexes. The relaxation parameters of other listed isostructural couples do not exhibit any reliable tendency upon the halide ligand replacement. On the other hand, the most apparent trend arisen upon the exchange of Cl$^-$ for Br$^-$ ligands across the listed isostructural couples is the decrease of the relaxation time. In other words, the bromido complexes show a faster relaxation of magnetization comparing to their isostructural chlorido analogues, regardless of the geometry of pentacoordinate polyhedra.

Patterning and sublimation deposition

The solution processability of **1-4** compounds was assessed by drop casting and lithographically controlled wetting (LCW), which is a wet-lithographic technique that exploits self-organization properties of materials in confinement successfully used for a variety of multifunctional materials, including complexes.[52-57] Figure S5 shows a scheme of the process, while detailed description and protocol are reported in ref. 58. All compounds exhibit similar behavior (see also Figure S43) thus we focused our attention, in the text, to compound **3** that we considered representative for the compounds subject of this article. Figure 8 shows typical optical and AFM images of drop cast film patterned structure of compound **3**. We chose the pattern parallel micrometric stripes, thus optically accessible, because this kind pattern is largely used to prove the processability and allow a direct comparison with drop cast films.[58] Compound **3** forms platted crystals randomly oriented on the surface that exhibit a clear birefringence when observed with polarized optical microscope (Figure 8a). Crystals appear homogeneously colored and extinguish when are oriented 45° with respect the polars orientation (Figure 8b). This behavior suggests that each crystal is formed by a single domain or by domains with the same orientation.

Printed stripes (Figure 8c) show moderate birefringence, probably due to the small thickness of the stripes. The stripes appear homogeneously colored in blue indicating that their mean thickness is constant over the entire stripe as also confirmed by AFM characterization. The stripes extinguish in four positions at intervals of 90°. This occurrence suggests that the crystalline domains are grown with the same orientation inside each stripe. Thus, we can deduce that the confined deposition by LCW has induced a coherent, long-range order along the direction of the stripes. No relevant quantity of material was observed in between the stripes by AFM. Although the morphology of printed stripes is imposed by the presence of the stamp protrusion during the fabrication, AFM images show the presence of the typical terraces of crystals inside the stripes.

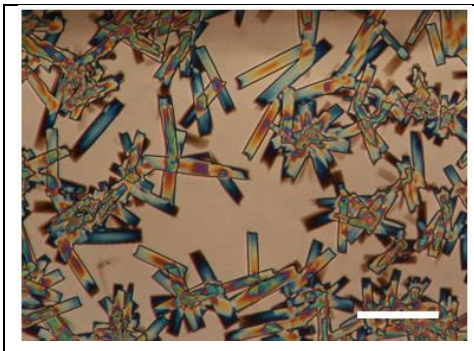

a)

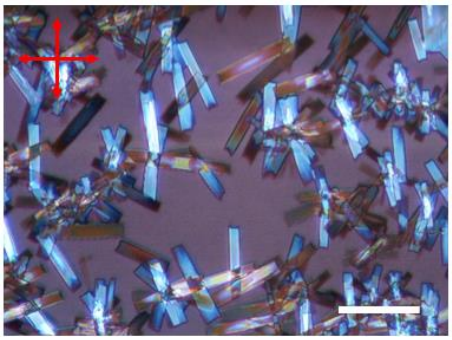

b)

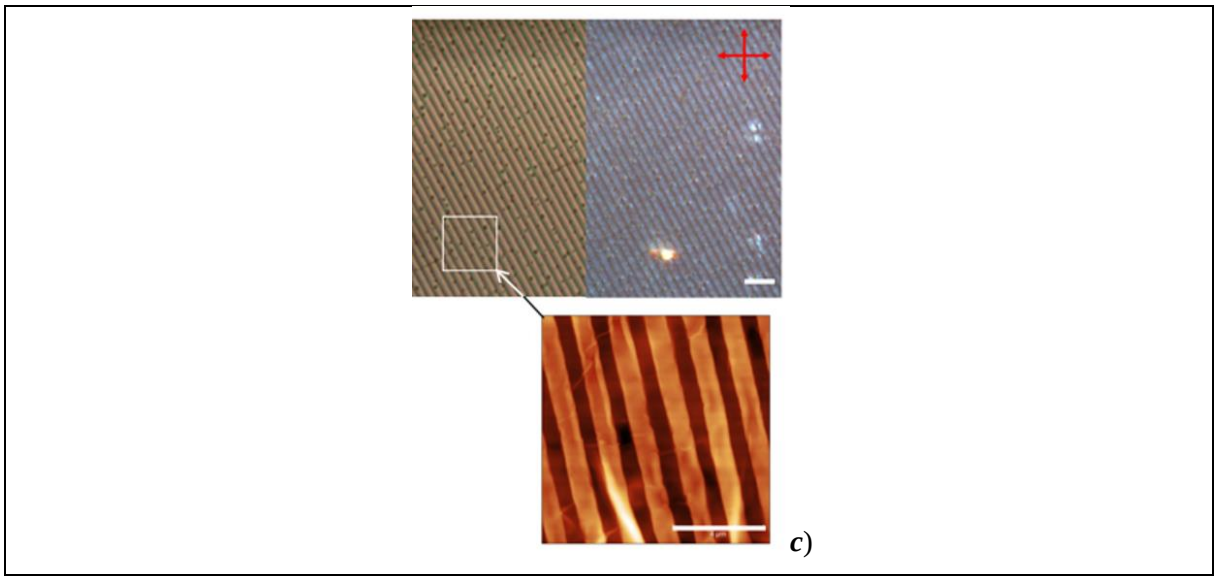

Figure 8 Thin deposit of **3** grown by drop casting on silicon surface: ***a***) optical micrographs taken under unpolarized light; ***b***) micrographs taken with crossed polars oriented along the axes of the image (bar is 20 µm) and ***c***) corresponding AFM image (z scale 0-550 nm, bar is 4 µm).

To have the full picture about the deposition possibilities of these SIMs we tested thermal sublimation of **1** and **2** onto silicon wafer and golden substrate. We chose these two to probe whethere there is any difference between chlorinated and brominated compound when it comes to the sublimation. For the deposition we used a home-built high-vacuum sublimation chamber equipped with a quartz crucible heated by silicon nitride heater and a thermocouple in thermal contact with the crucible with base pressure of 1×10^{-6} mbar in the chamber. Both **1** and **2** started to sublime in the 350 - 370 °C range. We chose X-ray photoelectron spectroscopy (XPS) as surface sensitive method to probe whether compounds stay intact after sublimation on surface by comparing the as-synthesized bulk powder, powder after sublimation at 370 °C and deposited samples. Further details can be found in ESI Figures (S44-S51). The absence of Co 2p, Cl 2p, and Br 3d photoelectron peaks on surfaces led us to suggestion that partial decomposition of the complex during the sublimation deposition process occurs. Therefore, for this type of compounds the wet-chemistry approach by LCW appears to be a better choice compared to thermal sublimation as the compounds undergo a partial decomposition.

Conclusions

In summary, we have prepared novel tridentate ligands - 2,6-bis(bezimidazole-1*H*-yl)pyridine derivatives decorated with aliphatic octyl or dodecyl substituents and used them for the synthesis of pentacoordinate Co(II) SIMs, suitable for the surface deposition by lithography techniques. The structural analysis confirmed mononuclear Co(II) complexes **1**-**4** with square planar coordination polyhedra which consist of three nitrogen donor atoms of corresponding tridentate ligand and two chlorido or bromido terminal ligands. Bromido and chlorido complexes containing the octyl or dodecyl decorated tridentate ligands form two isostructural couples **1**-**2** and **3**-**4** which differ on the type of used

halido terminal ligand. Furthermore, the temperature variable structural investigation revealed reversible crystallographic phase transition in complex **2** existing in low and high-temperature triclinic phases. Theoretical analysis revealed, that the distortion of the coordination environment has a profound effect on the ground electronic state of the complexes: while in the case of **2HT** and **4** the ground state is double degenerate, it is non-degenerate in other systems. Interestingly, the temperature-induced phase transition **2-LT** to **2-HT** leads to change of the ground state from $^4A_2$ to ^4E which is visible as an increase of its magnetic moment. All studied systems show magnetic anisotropy and spin Hamiltonian appears as a reasonable choice for interpretation of their static magnetic properties. Based on the extraction of the model parameters from CASSCF-NEVPT2+SOI analysis, the anisotropy can be called triaxial in the case of compounds **1**, **2LT**, and **2HT** with the shorter octyl substituents and axial in the second isostructural couple **3** and **4** containing tridentate ligand with dodecyl substitutents. On the other hand, the triaxial anisotropy can not be well identified by visual inspeciton of pictures of orientational dependence of molecular magnetization constructed from all eigenstates of CASSCF-NEVPT2+SOI wavefunction. At best, within this latter strategy, static magnetism of all systems can be identified as axial-like. EPR study revealed extreme anisotropy of the *g*-tensor components of the ground Kramers doublet, especially for compounds **3** and **4** showing an axial anisotropy, while strong rhombicity was observed for **1** and **2**. Furthermore, the magnetic anisotropy was investigated also by FIRMS, which revealed a good match with the values of axial and ekvatiorial ZFS parameters obtained from magnetic and *ab initio* study. Based on the AC susceptibility investigations, all four compounds are field-induced SIMs. The analysis of dynamic magnetic properties of the isostructural complexes **1** and **2** revealed a rare type of relaxation with two channels allocated frightfully close to each other. On the other hand, the relaxation in the second isostructural couple **3** and **4** is mediated through the single-channel, and analysis of the temperature evolution of relaxation time suggests that the replacement of the chlorido for bromido ligands accelerates the slow relaxation of magnetization. Additionally, the solubility of the reported Co(II) SIMs has enabled the fabrication of microstructured films on technological relevant substrates by an easy-to-handle and low cost wet lithographic technique.

Acknowledgement

Grant Agencies (Slovakia: APVV-18-0197, APVV-18-0016, APVV-19-0087, VEGA 1/0125/18, KEGA 018-STU-4) are acknowledged for the financial support. This article was written thanks to the generous support under the Operational Program Integrated Infrastructure for the project: "Strategic research in the field of SMART monitoring, treatment and preventive protection against coronavirus (SARS-CoV-2) ", Project no. 313011ASS8, co-financed by the European Regional Development Fund. I.Š. acknowledges the financial support from institutional sources of the Department of Inorganic Chemistry, Palacký University Olomouc, Czech Republic and to Ministry of Education, Youth and Sports of the Czech Republic under the project CEITEC 2020 (LQ1601). This article was also created with the support of the MŠVVaŠ of the Slovak Republic within the Research and Development Operational Program for the project “University Science Park of STU Bratislava” (ITMS project no. 26240220084) co-funded by the European Regional Development Fund. J.P. is grateful to the HPC center at the Slovak University of Technology in Bratislava, which is a part of the Slovak Infrastructure

of High Performance Computing (SIVVP project, ITMS code 26230120002, funded by the European region development funds, ERDF), for the computational time and resources made available. J.J. acknowledges the financial support from the internal grant of Brno University of Technology CEITEC VUT-J-20-6512. Furthermore, CzechNanoLab project LM2018110 funded by MEYS CR is gratefully acknowledged for the financial support of the measurements/sample fabrication at CEITEC Nano Research Infrastructure. J.D.M. acknowledges for the financial support of Brno PhD Talent 2018 scholarship. J. H. and J.D.M. acknowledges funding from MŠMT LTAUSA19060 project in the INTER-EXCELLENCE programme. Authors acknowledte prof. Jaromír Marek for the single-crystal data collection for compound **3** and prof. J. Kuchár for the temperature dependent diffraction measurements of **2**.

References

1. Sessoli, R.; Gatteschi, D.; Caneschi, A.; Novak, M. A. Magnetic bistability in metal ion cluster 1993, 365, 141-143.
2. Sessoli, R. Nanoscience: Single-atom data storage. Nature 2017, 543 (7644), 189 − 190.
3. Natterer, F. D.; Yang, K.; Paul, W.; Willke, P.; Choi, T.; Greber T.; Heinrich, A. J.; Lutz, C. P. Reading and writing single-atom magnets. Nature 2017, 543 (7644), 226 − 228.
4. Baumann, S.; Paul, W.; Choi, T.; Lutz, C. P.; Ardavan, A.; Heinrich, A. J. Electron paramagnetic resonance of individual atoms on a surface. Science 2015, 350 (6259), 417 − 420.
5. Sessoli, R.; Tsai, H. L.; Schake, A. R.; Wang, S.; Vincent, J. B.; Folting, K.; Gatteschi, D.; Christou, G.; Hendrickson, D. N. High-spin molecules: [Mn12O12(O2CR)16(H2O)4]. J. Am. Chem. Soc. 1993, 115, 1804 − 1816.
6. Ako, A. M.; Hewitt, I. J.; Mereacre, V.; Clérac, R.; Wernsdorfer,W.; Anson, C. E.; Powell, A. K. A Ferromagnetically Coupled Mn19 Aggregate with a Record S = 83/2 Ground Spin State. Angew. Chem., Int. Ed. 2006, 45, 4926 − 4929.
7. Dey, A.; Kalita, P.; Chandrasekhar, V. Lanthanide(III)-Based Single-Ion Magnets, ACS Omega 2018, 3, 9462 – 9475.
8. Rechkemmer, Y.; Breitgoff, F. D.; van der Meer, M.; Atanasov, M.; Hakl, M.; Orlita, M.; Neugebauer, P.; Neese, F.; Sarkar, B.; van Slageren, J. A four-coordinate cobalt(II) single-ion magnet with coercivity and a very high energy barrier, Nature commun., 2021, 7, 10467.
9. Ed. Layfield, R. A.; Murugesu, M.: Lanthanides and Actinides in Molecular Magnetism, Wiley-VCH Verlag GmbH & Co. KGaA, Weinheim, 2015.
10. Guo, F-S; Day, B. M; Chen, Y-C.; Tong, M-L.; Mansikkam-ki, A.; Layfield, R. A. A Dysprosium Metallocene Single-Molecule Magnet Functioning at the Axial Limit. Angew. Chem. Int. Ed. 2017, 56, 11445 –11449
11. Goodwin, C.A.P.; Ortu, F.; Reta, D.; Chilton, N. F.; Mills, D. P. Molecular magnetic hysteresis at 60 Kelvin in dysprosocenium. Nature 2017, 548, 439.
12. Guo, F-S; Day, B. M; Chen, Y-C.; Tong, M-L.; Mansikkam-ki, A.; Layfield, R. A. Magnetic hysteresis up to 80 Kelvin in a dysprosium metallocene single-molecule magnet. Science 2018 362, 1400-1403.
13. Frost, J. M.; Harriman, K. L. M.; Murugesu, M. The rise of 3-d single-ion magnets in molecular magnetism: towards materials from molecules? Chem. Sci. 2016, 7 (4), 2470 − 2491.
14. Craig, G. A.; Murrie, M. 3d single-ion magnets. Chem. Soc. Rev. 2015, 44 (8), 2135 − 2147.
15. Ghosh, S.; Kamilya, S.; Das, M.; Mehta, S.; Boulon, M-E.; Nemec, I.; Rouzières, M.; Herchel, R.; Mondal, A. Effect of Coordination Geometry on Magnetic Properties in a Series of Cobalt(II)

Complexes and Structural Transformation in Mother Liquor. Inorg. Chem. 2020, 59, 7067 – 7081. J. Am. Chem. Soc. 2011, 133, 15814 – 15817.

16. Jurca, T.; Farghal, A.; Lin,P-H.; Korobkov, I.; Murugesu, M., Richeson D. S. Single-Molecule Magnet Behavior with a Single Metal Center Enhanced through Peripheral Ligand Modifications.
17. Mondal, A. K.; Goswami,T.; Misra, A., Konar, S. Probing the Effects of Ligand Field and Coordination Geometry on Magnetic Anisotropy of Pentacoordinate Cobalt(II) Single-Ion Magnets. Inorg. Chem. 2017, 56, 6870−6878.
18. Switlicka, A.S.; Machura, B.; Penkala, M.; Bienko, A.; Bienko, D.; Titiš, J.; Rajnak, C.; Boča, R.; Ozarowski, A.; Ozerov, M. Slow Magnetic Relaxation in Cobalt(II) Field-Induced Single-Ion Magnets with Positive Large Anisotropy. Inorg. Chem. 2018, 57, 12740−12755.
19. Brachňaková, B.; Matejová, S.; Moncoľ, J.; Herchel, R.; Pavlik, J.; Moreno-Pineda, E.; Ruben, M.; Šalitroš, I. Dalton Trans. Stereochemistry of coordination polyhedral vs. single ion magnetism in penta- and hexacoordinated Co(II) complexes with tridentate rigid ligands, 2020, 49, 1249-1264.
20. Holmberg, R. J.; Murugesu, M. Adhering magnetic molecules to surfaces. J. Mat. Chem. C 2015 3, 11986.
21. Hruby, J.; Vavreckova, S.; Masaryk, L.; Sojka, A.; Navarro-Giraldo, J.; Bartos, M.; Herchel, R.; Moncol, J.; Nemec, I.; Neugebauer, P. Deposition of Tetracoordinate Co(II) Complex with Chalcone Ligands on Graphene. Molecules, 25, 5021.
22. Cañon-Mancisidor, W.; Miralles, S. G., Baldoví, J. J.; Mínguez Espallargas, G., Gaita-Ariño, A., Coronado, E. Sublimable Single Ion Magnets Based on Lanthanoid Quinolinate Complexes: The Role of Intermolecular Interactions on Their Thermal Stability. Inorg. Chem. 2018, 57, 14170-14177.
23. Miralles, S. G.; Bedoya-Pinto, A.; Baldov,J. J.; Mancisidor, W. C.; Prado, Y.; Prima-Garcia, H.; Gaita-Arino, A.; Mínguez Espallargas, G.; Hueso, L. E., Coronado, E. Sublimable chloroquinolinate lanthanoid single-ion magnets deposited on ferromagnetic electrodes. Chem. Sci., 2018, 9, 199-208.
24. Saywell, A.; Magnano, G.; Satterley, C. S.; Perdigão, L. M. A.; Britton, A. J.; Taleb, N.; Giménez-López, M. C.; Champness, N. R.; O'Shea, J. N.; Beton, P. H. Self-assembled aggregates formed by single-molecule magnets on a gold surface. Nature Commun. 2010, 1, 75.
25. Rozbořil, J.; Rechkemmer, Y.; Bloos, D.; Münz, F.; Wang, C. N.; Neugebauer, P.; Čechal, J.; Novák, J.; van Slageren J. Magneto-optical investigations of molecular nanomagnet monolayers. Dalton Trans., 2016, 45, 7555-7558.
26. Rajnák, C.; Titiš, J.; Šalitroš, I.; Boča, R.; Fuhr, O.; Ruben, M. Zero-field splitting in pentacoordinate Co(II) complexes. *Polyhedron* 2013, 65, 122-128
27. Nemec, I.; Heng, L.; Herchel, R.; Xuequan, Z.; Trávníček, Z. Magnetic anisotropy in pentacoordinate 2,6-bis(arylazanylidene-1- chloromethyl)pyridine cobalt(II) complexes with chlorido co-ligands. *Synth. Met.* 215 (2016) 158–163
28. Rajnák, C.; Titiš, J.; Miklovič, J.; Kostakis, G. E.; Fuhr, O.; Ruben, M.; Boča, R. Five mononuclear pentacoordinate Co(II) complexes with field-induced slow magnetic relaxation. *Polyhedron* 2017, 126, 174–183.
29. Cahier, B.; Perfetti, M.; Zakhia, G.; Naoufal, D.; El-Khatib, F.; Guillot, R.; Rivière, Sessoli, R.; Barra, A.-L.; Guihéry, N.; Mallah, T. Magnetic Anisotropy in Pentacoordinate NiII and CoII Complexes: Unravelling Electronic and Geometrical Contributions. Chem. Eur. J. 2017, 23, 3648-3657.
30. Mondal, A. K.; Jover, J.; Ruiz, E.; Konar, S. Investigation of easy-plane magnetic anisotropy in P-ligand square-pyramidal CoII single ion magnets. Chem. Commun. 2017, 53, 5338-5341.

31. Schweinfurth, D.; Krzystek, J.; Atanasov, M.; Klein, J.; Hohloch, S.; Telser, J.; Demeshko, S.; Meyer, F.; Neese, F.; Sarkar, B. Tuning Magnetic Anisotropy Through Ligand Substitution in Five-Coordinate Co(II) Complexes. Inorg. Chem. 2017, 56, 5253-5265.
32. Massoud, S. S.; Fischer, R. C.; Mautner, F. A.; Parfait, M. M.; Herchel, R.; Trávníček, Z. Pentacoordinate cobalt(II) complexes with neutral tripodal N-donor ligands: Zero-field splitting for a distorted trigonal bipyramidal geometry. Inorg. Chim. Acta 2018, 471, 630-639.
33. Cui, Y.; Xu, Y.; Liu, X.; Li, Y.; Wang, B.-L.; Dong, Y.; Li, W.; Lei, S. Field-Induced Single-Ion Magnetic Behavior in Two Mononuclear Cobalt(II) Complexes. Chem. Asian J. 2019, 14, 2620-2628.
34. Massoud, S. S.; Perez, Z. E.; Courson, J. R.; Fischer, R. C.; Mautner, F. A.; Vančo, J.; Čajan, M.; Trávníček, Z. Slow magnetic relaxation in penta-coordinate cobalt(II) field-induced single-ion magnets (SIMs) with easy-axis magnetic anisotropy. Dalton Trans. 2020, 49, 11715-11726.
35. Cui, H.-H..; Ding, M.-M.; Zhang, X.-D.; Lv, W.; Zhang, Y.-Q.; Chen, X.-T., Wang, Z.; Ouyang, Z.-W., Xue, Z.-L. Magnetic anisotropy in square pyramidal cobalt(II) complexes supported by a tetraazo macrocyclic ligand. Dalton Trans. 2020, 49, 14837-14846.
36. Damgaard-Møller, E.; Krause, L.; Lassen, H.; Malaspina, L. A.; Grabowsky, S.; Bamberger, H.; McGuire, J.; Miras, H. N.; Sproules, S.; Overgaard, J. Investigating Complex Magnetic Anisotropy in a Co(II) Molecular Compound: A Charge Density and Correlated Ab Initio Electronic Structure Study. *Inorg. Chem.* **2020**, 59, 13190-13200.
37. Boča, R. Magnetic Functions Beyond the Spin-Hamiltonian. Struct. Bond. 2006 117: 1-264.
38. Atanasov, M.; Ganyushin, D.; Sivalingam, K.; Neese, F. In *Molecular Electronic Structures of Transition Metal Complexes II*; Mingos, D. M. P., Day, P., Dahl, J. P., Eds.; Springer Berlin Heidelberg: Berlin, Heidelberg, **2012**; pp 149– 220.
39. Figgis, B. N.; Hitchman, M. A. Ligand Field Theory and Its Applications, Wiley-VCH, New York, 2000.
40. Banci, L.; Bencini, A.; Benelli, C.; Gatteschi, D.; Zanchini, C. Spectral-Structural Correlations in High-Spin Cobalt(II) Complexes. *Struct. Bond.* **1982**, 52: 37-86.
41. Mostafanejad, M. Basics of the Spin Haniltonian Formalism. *Int. J. Quantum Chem.* **2014**, 114, 1495-1512.
42. Legendre, C. M.; Damgaard-Møller, E.; Overgaard, J.; Stalke, D. The Qeust for Optimal 3 d Orbital Splitting inTetrahedral Cobalt Single-Molecule Magnets Featuring Colossal Anisotropy and Hysteresis. *Eur. J. Inorg. Chem.* **2021**, doi.org/10.1002/ejic.202100465
43. Damgaard-Møller, E.; Krause, L.; Tolborg, K.; Macetti, G.; Genoni, A.; Overgaard, J. Quantification of the Magnetic Anisotropy of a Single-Molecule Magnet from the Experimental Electron Density. *Angew. Chem. Int. Ed.* **2020**, *59*, 21203-21209.
44. Herchel, R.; Váhovská, L.; Potočňák, I.; Trávníček, Z. Slow Magnetic Relaxation in Octahedral Cobalt(II) Field-Induced Single-Ion Magnet with Positive Axial and Large Rhombic Anisotropy. *Inorg. Chem.* **2014**, 53, 5896-5898.
45. Stoll, S.; Schweiger, A. EasySpin, a comprehensive software package for spectral simulation and analysis in EPR. J. Magn. Reson. 2006, 178, 42–55. https://doi.org/10.1016/j.jmr.2005.08.013
46. Banci L., Bencini A., Benelli C., Gatteschi D., Zanchini C. (1982) Spectral-structural correlations in high-spin cobalt(II) complexes. In: Structures versus Special Properties. Structure and Bonding, vol 52. Springer, Berlin, Heidelberg. https://doi.org/10.1007/BFb0111296
47. Nehrkorn J, Holldack K, Bittl R, Schnegg A. Recent progress in synchrotron-based frequency-domain Fourier-transform THz-EPR. J. Magn. Reson. 2017, 280, 10–19. https://doi.org/10.1016/j.jmr.2017.04.001

48. Carlin, R.-L.; Magnetochemistry, Springer-Verlag, Berlin, 1986.
49. Singh, A.; Shrivastava, K. Optical-acoustic two-phonon relaxation in spin systems Phys. Status Solidi B, 1979.
50. Rajnák, C.; Varga, F.; Titiš, J.; Moncoľ, , J.; Boča, R. Field-Supported Single-Molecule Magnets of Type [Co(bzimpy)X2]. Eur. J. Inorg. Chem. 2017, 1915–1922.
51. Woods, T. J.; Ballesteros-Rivas, M. F.; Gomez-Coca, S.; Ruiz, E.; Dunbar, K. R. Relaxation Dynamics of Identical Trigonal Bipyramidal Cobalt Molecules with Di ff erent Local Symmetries and Packing Arrangements: Magnetostructural Correlations and *ab inito* Calculations. J. Am. Chem. Soc. 2016, 138, 16407−16416.
52. Cavallini, M.; Calo, A.; Stoliar, P.; Kengne, J.C.; Martins, S.; Matacotta, F.C.; Quist, F.; Gbabode, G.; Dumont, N.; Geerts, Y.H.; Biscarini, F. Lithographic Alignment of Discotic Liquid Crystals: A New Time–Temperature Integrating Framework. Adv. Mater. 2009, 21, 4688-4691.
53. Melucci, M.; Zambianchi, M.; Favaretto, L.; Palermo, V.; Treossi, E.; Montalti, M.; Bonacchi, S.; Cavallini, M. Chem. Commun. Multicolor, large-area fluorescence sensing through oligothiophene-self-assembled monolayers. 2011, 47, 1689-1691.
54. Cavallini, M.; Hemmatian, Z.; Riminucci, A.; Prezioso, M.; Morandi, V.; Murgia, M. Regenerable Resistive Switching in Silicon Oxide Based Nanojunctions. Adv. Mater. 2012, 24, 1197-1201.
55. Gentili, D.; Cavallini, M. Wet-lithographic processing of coordination compounds. Coor. Chem. Rev. 2013, 17-18, 2456-2467.
56. Gentili, D.; Valle, F.; Albonetti, C.; Liscio, F.; Cavallini, M. Self-Organization of Functional Materials in Confinement. Accounts of Chemical Research 2014, 47, 2692-2699.
57. Gentili, D.; Gazzano, M.; Melucci, M.; Jones, D.; Cavallini, M. Polymorphism as an additional functionality of materials for technological applications at surfaces and interfaces. Chem. Soc. Rev. 2019, 48, 2502-2517.
58. Cavallini, M.; Gentili, D.; Greco, P.; Valle, F.; Biscarini, F. Fluorescent labeling of nano-sized vesicles released by cells and subsequent quantitative and qualitative analysis by high-resolution flow cytometry. Nature Protocols 2012, 7, 1668-1676.